



## RESEARCH ARTICLE

10.1029/2020GB006671

### Key Points:

- We present a synoptic survey of radiocarbon content of dissolved and particulate organic carbon across the Mackenzie river basin
- This data reveal intriguing relationships between radiocarbon content and turbidity, water isotopes, and topography
- This study provides a road map of the key sources and controls of riverine OC age in this rapidly changing river basin

### Supporting Information:

- Supporting Information S1
- Tables S1–S4

### Correspondence to:

A. Campeau,  
audrey.campeau@slu.se

### Citation:

Campeau, A., Sørensen, A. L., Martma, T., Åkerblom, S., & Zdanowicz, C. (2020). Controls on the  $^{14}\text{C}$  content of dissolved and particulate organic carbon mobilized across the Mackenzie River basin, Canada. *Global Biogeochemical Cycles*, 34, e2020GB006671. <https://doi.org/10.1029/2020GB006671>

Received 25 MAY 2020

Accepted 15 NOV 2020

Accepted article online 25 NOV 2020

## Controls on the $^{14}\text{C}$ Content of Dissolved and Particulate Organic Carbon Mobilized Across the Mackenzie River Basin, Canada

A. Campeau<sup>1,2</sup> , A. L. Sørensen<sup>3,4</sup> , T. Martma<sup>5</sup> , S. Åkerblom<sup>6</sup> , and C. Zdanowicz<sup>1</sup>

<sup>1</sup>Department of Earth Sciences, Uppsala University, Uppsala, Sweden, <sup>2</sup>Now at Department of Forest Ecology and Management, Swedish University of Agricultural Sciences, Umeå, Sweden, <sup>3</sup>Department of Environmental Science and Analytical Chemistry, Stockholm University, Stockholm, Sweden, <sup>4</sup>Department of Environmental Research and Monitoring, Swedish Museum of Natural History, Stockholm, Sweden, <sup>5</sup>Department of Geology, Tallinn University of Technology, Tallinn, Estonia, <sup>6</sup>Statistiska Centralbyrån (SCB), Statistic Sweden, Stockholm, Sweden

**Abstract** The Mackenzie River Basin (MRB) delivers large quantities of organic carbon (OC) into the Arctic Ocean, with significant implications for the global C budgets and ocean biogeochemistry. The amount and properties of OC in the Mackenzie River's delta have been well monitored in the last decade, but the spatial variability in OC sources transported by its different tributaries is still unclear. Here we present new data on the radiocarbon ( $^{14}\text{C}$ ) content of dissolved and particulate OC ( $\Delta^{14}\text{C}$ -DOC and  $\Delta^{14}\text{C}$ -POC) across the mainstem and major tributaries of the MRB, comprising 19 different locations, to identify factors controlling spatial patterns in riverine OC sources. The  $\Delta^{14}\text{C}$ -DOC and  $\Delta^{14}\text{C}$ -POC varied across a large range, from  $-179.9\text{‰}$  to  $62.9\text{‰}$ , and  $-728.8\text{‰}$  to  $-9.0\text{‰}$ , respectively. Our data reveal a positive spatial coupling between the  $\Delta^{14}\text{C}$  of DOC and POC across the MRB, whereby the most  $^{14}\text{C}$ -depleted waters were issued from the mountainous west bank of the MRB. This  $^{14}\text{C}$ -depleted DOC and POC likely originates from a combination of petrogenic sources, connected with the presence of kerogens in the bedrock, and biogenic sources, mobilized by thawing permafrost. Our analysis also reveals intriguing relationships between  $\Delta^{14}\text{C}$  of DOC and POC with turbidity, water stable isotope ratio and catchment elevation, indicating that hydrology and geomorphology are key to understanding riverine OC sources in this landscape. A closer examination of the specific mechanisms giving rise to these relationships is recommended. For now, this study provides a road map of the key OC sources in this rapidly changing river basin.

## 1. Introduction

The Mackenzie River Basin (MRB) is the fourth largest source of freshwater to the Arctic Ocean. Its waters carry large quantities of organic carbon (OC), in both particulate (POC) and dissolved (DOC) forms, which has considerable implications for global C budgets and ocean biogeochemistry (Stein & Macdonald, 2004). The largest share of the MRB, which lies north of  $50^\circ\text{N}$ , has so far been only weakly affected by human activities or infrastructure development (e.g., agriculture, mines, and dams). However, the region is now experiencing one of the fastest rate of warming across the globe, with the Mackenzie River delta having warmed by  $\sim 3^\circ\text{C}$  ( $>4.5^\circ\text{C}$  in winter) since the midtwentieth century (Bush & Flato, 2019). This warming is now profoundly transforming the landscape and hydrology of the MRB through accelerated thawing of permafrost, thermokarst development, riverbank slumping, greater forest fire activity and a northward migration of the tree line (Burn & Kokelj, 2009; Guay et al., 2014; St. Jacques & Sauchyn, 2009). Such environmental changes have increased the riverine DOC export from the MRB by  $\sim 39\%$  over the past half century (Tank et al., 2016). Monitoring conducted near the mouth of the Mackenzie River since 2003 by the Arctic Great Rivers Observatory (ArcticGRO; Holmes et al., 2020) has documented interannual and seasonal variations in OC export from the MRB (Goñi et al., 2005; Guo et al., 2007; Raymond et al., 2007). However, the sources of OC mobilized by its different tributaries, together with their spatial controls, remain to be fully resolved.

The radiocarbon content ( $\Delta^{14}\text{C}$ ) can provide information about the sources of OC transported in rivers. This can be particularly useful in landscapes like the MRB, where riverine OC may originate from a mixture of

©2020. The Authors.

This is an open access article under the terms of the Creative Commons Attribution License, which permits use, distribution and reproduction in any medium, provided the original work is properly cited.

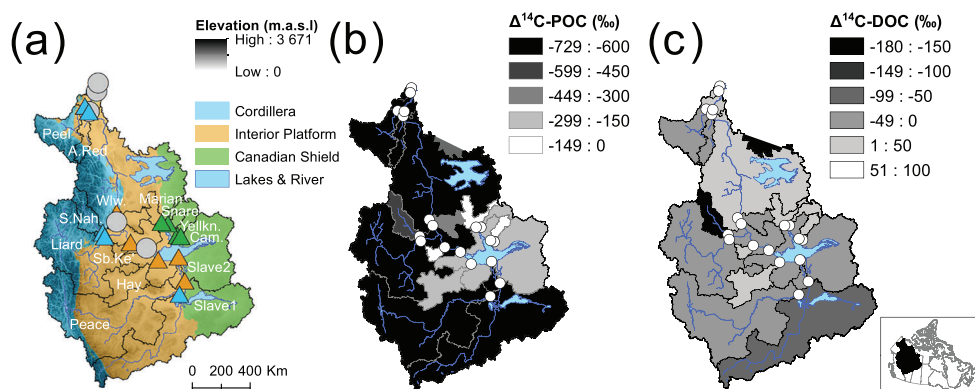


**Figure 1.** Maps of the Mackenzie River Basin (MRB) (a) the area of each geological regions (Cordillera [blue], Interior Platform [orange], and Canadian Shield [green]), with elevation displayed as background shading. The symbols indicate the river sampling location for tributaries (triangles color coded by region as in legend) and along the mainstem of the Mackenzie River (gray circles). Tributaries have their upstream catchment area delineated with black lines and overlaying their abbreviated names. The maps in (b) and (c) illustrates the  $\Delta^{14}\text{C}$ -POC and  $\Delta^{14}\text{C}$ -DOC data, respectively. The catchment area upstream of each river sampling location was shaded according to the  $\Delta^{14}\text{C}$ . Darker shades indicate older OC (i.e.,  $\Delta^{14}\text{C}$ -depleted) and lighter shades indicate younger OC (i.e.,  $\Delta^{14}\text{C}$  enriched). White circles indicate the water sampling location. Major lakes and rivers are illustrated in blue on all maps to serve as reference.

sources that spans a large range in age. These sources comprises ancient OC, present both in the bedrock (petrogenic C; e.g., from coal or shales) and in soils and surficial sediments (biogenic C; e.g., in permafrost and peatlands), and also young OC, derived from terrestrial and aquatic primary production. Warming in the MRB can potentially alter riverine OC sources through an increased export of ancient OC, associated with rapidly growing retrogressive thaw slumps (Lacelle et al., 2015; Lantz & Kokelj, 2008; Littlefair et al., 2017) and deepening of the active layer in ice-rich permafrost areas (Abbott et al., 2016; Aiken et al., 2014; Feng et al., 2013) or increase the export of younger-OC, resulting from enhanced terrestrial and aquatic primary production (Finstad et al., 2016; Qian et al., 2010).

The  $\Delta^{14}\text{C}$  analysis of riverine OC, carried out on samples collected from the mouth of the Arctic Great Rivers (Holmes et al., 2020) has revealed that the MRB exports on average the oldest POC (i.e.,  $^{14}\text{C}$  depleted) to the Arctic Ocean out of all Arctic Great Rivers, but also a mixture of aged and modern DOC (Holmes et al., 2020; Raymond et al., 2007). The prevailing hypothesis explaining these age patterns is that POC is mostly derived from petrogenic sources (Hilton et al., 2015; Horan et al., 2019) and thawing permafrost and river bank erosion (Feng et al., 2013; Vonk et al., 2015; Wild et al., 2019), while DOC contains a comparatively larger proportion of recent photosynthates derived from terrestrial vegetation (Guo et al., 2007; Marwick et al., 2015). At present, the range and variability in riverine  $\Delta^{14}\text{C}$ -OC is unknown in large parts of the MRB, partly owing to the remoteness of the region and the limited network of roads allowing access to the rivers. This limits our understanding of the processes regulating OC export in this river catchment and how these may evolve under rapidly changing hydro-climatic conditions in the region.

In order to better define the sources of riverine OC and their controls across the MRB, we conducted a synoptic survey of the  $\Delta^{14}\text{C}$  of riverine DOC and POC in 14 of its different tributaries and five different locations along the Mackenzie River itself. In addition, we also determined the stable isotope ratio of river water ( $\delta^{18}\text{O}$ ), as well as a suite of water chemistry variables (including pH, conductivity, turbidity, nitrogen, and major cations) at these same locations. We further compiled geospatial data to identify properties of different sub-basins that could explain the spatial patterns in riverine  $\Delta^{14}\text{C}$ -OC seen in our samples.

## 2. Materials and Methods

### 2.1. The Mackenzie River Basin

The MRB is the largest river basin in Canada. Its watershed covers an area of  $1.7 \times 10^6 \text{ km}^2$ , stretching across three distinct geological regions; (from west to east) the Cordillera (24%), the Interior Platform (53%), and the Canadian Shield (23%) (Figure 1). The Cordillera, comprising the Rocky Mountains, is characterized by high elevation (mean 1,187 m.a.s.l), steep topographic gradients (mean slope  $11.1^\circ$ ) and thin surficial

deposits (mean depth 3 m) (Figure 1 and Table S1 in the supporting information). The Interior Platform has a mean elevation of 459 m.a.s.l, a flat topography (mean slope 1.4°), and is often covered with thick surficial deposits (mean depth 28 m) (Figure 1 and Table S1). The Canadian shield is also characterized by low elevations (mean 355 m.a.s.l.) and a similarly flat topography (mean slope 1.4°) but has much thinner surficial deposits (mean depth 10 m) than the Interior Platform (Figure 1 and Table S1).

Most of the MRB lies southward of the tree line. Coniferous forest makes up the majority of the land cover, although there are occurrences of mixed and deciduous forest in the southern part of the Interior Platform. Lakes are most abundant in the Canadian Shield (27%), while wetlands are equally distributed between the Canadian Shield and Interior Platform (3% each; Table S1; Latifovic et al., 2017). The Cordillera contains a few occurrences of glaciers (1%), mostly in the headwaters of the South Nahanni River (Table S1 and Figure S1a; Latifovic et al., 2017). Urbanization and agriculture are mostly confined to the southern part of the Interior Platform (Peace and Athabasca sub-basins), together comprising 2% of the MRB (Table S2; Latifovic et al., 2017). Flow in the Peace River is regulated by hydroelectric dams, including the W. A. C. Bennett Dam and the Peace Canyon Dam. There are three large lakes in the MRB, from south to north: Lake Athabasca, Great Slave Lake, and Great Bear Lake (Figure 1). The Mackenzie River proper begins at the outlet of Great Slave Lake and terminates in a broad delta on the shores of the Beaufort Sea.

All three geological regions within the MRB comprise sedimentary or metasedimentary rocks, some of which are a source of ancient petrogenic OC, such as kerogens (Figure S1a and Table S1). The largest potential source-areas for the Mackenzie River are shale and coal deposits of Devonian to Carboniferous age in the central Mackenzie River valley and in the Liard Basin (Interior Platform and Cordilleran foreland; Cameron & Beaton, 2000). Coal deposits of Cretaceous age in the Peace River sub-basin also contribute petrogenic OC in the southernmost part of the MRB (Jautzy et al., 2015). The Canadian Shield contains large areas of granitoids and gneiss containing no ancient OC, which is interspersed with Archean to Precambrian metasedimentary rocks (Table S1). Glacial sediments make up the majority of the surface materials across the MRB, but the Cordillera and Canadian Shield also contain vast areas of exposed bedrock (Table S1; Fulton, 2014; Pelletier et al., 2016). Soil OC accumulation in the MRB has been ongoing since Late Pleistocene deglaciation, with peatland initiation reaching its peak between 8 and 7 ka BP, and permafrost aggradation occurring in the mid- to late Holocene, between ~6 and 1 ka BP (Gorham et al., 2007; Treat & Jones, 2018). Peat-rich soils, with an OC content >50%, comprise 18% of the Interior Platform, compared with 0.01 and 0.07% of the Canadian Shield and Cordillera respectively (Figure S1b; Xu et al., 2018). Continuous and discontinuous permafrost occurs mostly along the northeastern part of MRB, comprising 50% of the total catchment area (Figure S1c and Table S1). Most permafrost in the Cordillera and Canadian Shield has a thin overburden and a low ice content, while the permafrost areas in the Interior Platform are often under thick overburden and may contain massive ground ice, as for example in the Mackenzie River delta (Table S1; Brown et al., 2002).

## 2.2. Water Sampling

Our survey was carried out between the 8th–30th of June 2018. Spring freshet typically occurs during this period, which corresponds to peak discharge and therefore the most important period of the year in terms of OC delivery to the Arctic Ocean (e.g., ~60% for DOC; Raymond et al., 2007). Samples were often collected slightly before peak discharge (hydrograph for the Mackenzie, Liard, and Peace Rivers is presented in Figure S2). Sampling was carried out from south to north, following the normal sequence of seasonal river ice break-up; beginning south of Great Slave Lake in early June, and ending in the Mackenzie River delta region at the end of the month. A single depth-integrated water sample was collected from each location. At most locations, water samples were collected in mid-channel off a boat's prow. When a safe access on the river by boat was impossible, water samples were collected instead in the shallow depths a few meters off the shore (samples offshore are marked on Figure S3 and Table S2).

The depth-integrated water sample was collected using suspended sediment samplers models D95 (mid-channel sampling) or D81 (nearshore sampling) developed by the U.S. Federal Interagency Sedimentation Project (Davis, 2005). Samplers were fitted with a 1 L polytetrafluoroethylene (PTFE) bottle, which was thoroughly rinsed with river water at each site prior to sampling. Water was collected at discrete depth increments of ~1 m (or less in shallower waters), down to just above the channel bed, or to a maximum depth of 5 m, to obtain depth-integrated water samples (Table S2). The deepest waters were incorporated in

several samples, but not in others (full-depth profile samples are marked on Figure S3). Each 1 L increment was poured into a pre-acid-washed, 14-L high-density polyethylene (HDPE) churn (Bel-Art Products, Wayne, NJ, USA). Once back to shore, this composite sample was divided into sub-samples for various water chemistry analyses. At each location, water temperature, pH, oxygen saturation and turbidity were measured in situ, generally at a depth ranging between 0.15 to 2 m from the surface, using a submersible probe (YSI Instruments, Yellow Springs, OH, USA).

### 2.3. Carbon Isotope Analyses

For analysis of the  $\Delta^{14}\text{C}$ -DOC and  $\Delta^{14}\text{C}$ -POC, sub-samples of water were filtered on site through pre-baked quartz microfiber filters with a diameter of 25 mm (Whatman grade QM-A, GE Healthcare, Chicago, IL, USA) in a closed tubing circuit using a portable peristaltic pump (Geotech Geopump™ Series II; Geotech Environmental Equipment, Inc., Denver, CO, USA). The filter used have a reported nominal retention efficiency of 99% for liquid suspensions of particles with diameters  $\geq 2.2\ \mu\text{m}$ . Measurements of DOC in sample water filtered through the QM-A filters and through polyethersulfone membranes with  $0.45\ \mu\text{m}$  pore diameters were in very close agreement, indicating that the QM-A filters were highly efficient for sub-micron OC particles (Tables S2 and S3). The water filtered for  $\Delta^{14}\text{C}$ -DOC was collected in sterile 1 L Nalgene HDPE bottles, while the filters for  $\Delta^{14}\text{C}$ -POC were placed inside sterile petri dishes and sealed in polyethylene bags during road transport. The filters were subsequently dried overnight in an oven at  $50^\circ\text{C}$  at the Taiga Environmental Laboratory in Yellowknife, or at the Western Arctic Research Center in Inuvik. Some major tributaries of the Mackenzie River carry very turbid waters during the high flow season (100 to  $>400$  NTU), which made on-site filtering challenging. At such sites, the sub-samples were bottled without filtration, to be later filtered two weeks later in the laboratory (samples with delayed filtration are marked on Figure S3). This was the case for both sampling locations along the Slave River, the Arctic Red River and the Mackenzie River in Inuvik (Table S2). Delays in filtrations could have influenced the OC concentrations and  $\Delta^{14}\text{C}$  content in these samples. However, measurements from the Mackenzie River in Inuvik did not differ significantly from these of other samples collected along the Mackenzie River, indicating a negligible skew in the OC concentrations and  $\Delta^{14}\text{C}$  content due to delayed filtrations (Figure S3).

The  $\Delta^{14}\text{C}$ -DOC and  $\Delta^{14}\text{C}$ -POC in the water samples were determined at the A. E. Lalonde Accelerator Mass Spectrometry Laboratory of the University of Ottawa, as described in Crann et al. (2017) and St-Jean et al. (2017). Sample pre-treatment to remove inorganic carbon from carbonates was done with HCl for POC, and with  $\text{H}_3\text{PO}_4$  for DOC, following a wet oxidation technique based on Zhou et al. (2015) and Lang et al. (2016). The  $\text{CO}_2$  evolved from DOC or POC was then cryogenically purified on a vacuum extraction line, and the  $^{14}\text{C}/^{12}\text{C}$  ratio in  $\text{CO}_2$  was determined on a 3MV tandem accelerator mass spectrometer (High Voltage Engineering, Amersfoort, the Netherlands). Three blank quartz filters with known masses of  $^{14}\text{C}$ -free acetanilide were analyzed along with samples, and the released carbon mass ( $m_{\text{C}}$ ) and  $\Delta^{14}\text{C}$  on these were used to correct the sample  $\Delta^{14}\text{C}$  values using a mass balance method (e.g., Roberts et al., 2019) (Table S3). Total analytical uncertainties ( $2\sigma$ ) on individual  $\Delta^{14}\text{C}$  values ranged between 1.88–6.38‰ (median 3.95‰), which correspond to relative uncertainties of 0.3–6.0%, with the exception of a single sample (NT18-1; Cameron River), in which the uncertainty was much larger (43.8%) owing to its low OC content (Table S3).

Results are reported here as  $\Delta^{14}\text{C}$  values in ‰, which expresses the relative difference in  $^{14}\text{C}$  activity between the *absolute international standard* (base year 1950) and the sample activity corrected for age and normalized to  $\delta^{13}\text{C} = 25\text{‰}$  (Stuiver & Polach, 1977). The measured  $\Delta^{14}\text{C}$ -DOC and  $\Delta^{14}\text{C}$ -POC in each sample are in effect weighted averages for a mixture of OC components with possibly different  $^{14}\text{C}$  contents. Apparent mean  $^{14}\text{C}$  ages expressed in calendar years were omitted from the text to avoid misinterpretation, but these values are still listed in supplementary data together with fraction of modern carbon ( $F^{14}\text{C}$ ) (Table S3). For simpler communication of the results, we refer to more  $\Delta^{14}\text{C}$ -depleted samples as “Aged” or “old” and more  $\Delta^{14}\text{C}$  enriched as “young” or “modern.” Radiocarbon age calibration was performed using OxCal v4.3 (Ramsey, 2009).

For determination of the stable carbon isotope ratio of total OC ( $\delta^{13}\text{C}$ -TOC), unfiltered sub-samples were collected into TraceClean 40 mL borosilicate vials with silicon-PTFE septa, following standard methods of the U.S. Environmental Protection Agency (EPA). The  $\delta^{13}\text{C}$ -TOC were determined at the Jan Veizer Stable Isotope Laboratory of the University of Ottawa, on a OI Analytical model 1,030 wet TOC analyser

interfaced to a Thermo Finnigan DeltaPlus XP isotope ratio mass spectrometer. Calibration was performed using two different internal organic standards, prepared in solution three days before beginning analysis (St-Jean, 2003).

#### 2.4. Basic Water Properties

Basic physical and chemical properties of the water samples were measured at Taiga Environmental Laboratory, operated in Yellowknife by the Northwest Territories Government's Department of Environment and Natural Resources. Among the parameters measured were; pH, specific conductivity (SC), turbidity, total dissolved solids (TDS), total suspended solids (TSD), alkalinity, DOC, and TOC, dissolved and total nitrogen and the concentration of six major ionic species ( $\text{Ca}^{2+}$ ,  $\text{K}^+$ ,  $\text{Na}^+$ ,  $\text{Mg}^{2+}$ , and  $\text{SO}_4^{2-}$ ) (Table S2). The DOC and TOC concentrations were measured on a Shimadzu TOC/DOC analyzer, and the major ions on a Thermo Fisher Dionex ICS 5000 ion chromatography system (Table S2). POC concentrations were derived by subtracting the DOC fraction from the TOC concentrations. This introduces a fairly large uncertainty on the POC concentration measurements such that these data should be regarded with caution. All measurements of basic water properties were performed as per standard U.S. EPA methods and the Standard Methods for the Examination of Water and Wastewater (Rice et al., 2017). The stable isotope ratio of O and H in water ( $\delta^{18}\text{O}$  and  $\delta^2\text{H}$ ) in filtered samples was determined at the Institute of Geology of Tallinn's University of Technology, Estonia, by laser spectroscopy, using a Picarro model L2120-i water isotope analyzer (Picarro Inc., Sunnyvale, USA), which allows for the simultaneous determinations of  $^{18}\text{O}/^{16}\text{O}$  and  $^2\text{H}/^1\text{H}$  in  $\text{H}_2\text{O}$  (Lis et al., 2008) (Table S2). Results are reported relative to the Vienna Standard Mean Ocean Water with an analytical precision was  $\pm 0.1\text{‰}$  and  $\pm 1\text{‰}$  ( $1\sigma$ ) for  $\delta^{18}\text{O}$  and  $\delta^2\text{H}$ , respectively.

#### 2.5. Geographic and Statistical Analysis

The catchment area upstream of each sampling location was determined using the hydrology toolbox on ArcGIS 10.7. These areas were computed from the void-filled Canadian digital elevation model (CDEM; <http://ftp.geogratis.gc.ca>), with a spatial resolution of  $100\text{ m}^2$ , following aggregation of the original  $20\text{ m}^2$  resolution data. Stream lines were drawn using a  $1\text{ km}^2$  threshold on the derived flow accumulation raster, with which Strahler Stream Orders were determined for each location. The CDEM was also used for calculation of the mean elevation and slope of each sub-catchment. Other geospatial information that were obtained for each sub-basin included permafrost and ground ice coverage (Brown et al., 2002), land cover classes (Latifovic et al., 2017), bedrock type (Wheeler et al., 1996), surface material type (Fulton, 2014), soil thickness (Pelletier et al., 2016), and peatland cover (Xu et al., 2018). All geospatial data were projected using the Lambert Conformal Conic projection. Geospatial variables tested for significant relationships against  $\Delta^{14}\text{C}$ -DOC and  $\Delta^{14}\text{C}$ -POC include: total catchment area, stream order, total stream length, mean soil thickness, slope, and fraction for different land cover classes, bedrock geology types, surficial material types, permafrost, and ground ice types/content.

Nonparametric pairwise comparisons were performed using Dunn's test with Bonferroni corrections to determine statistically significant differences in  $\Delta^{14}\text{C}$ -DOC and  $\Delta^{14}\text{C}$ -POC between the three different geological regions. River samples were separated into three categories based on the fraction of catchment areas within each geological region. Tributaries associated with the Canadian Shield have their full catchment area located in that geological region. These tributaries include the Cameron, Snare, Marian, and Yellowknife River. Tributaries were associated with the Cordillera if they have their headwaters in this region, comprising  $>25\%$  of their catchment area. These tributaries include the Peace, Liard, South Nahanni, Arctic Red, and Peel River. Tributaries such as the Smbaa K'e, Willowlake, and Hay River, as well as the Slave River at Fort Fitzgerald and upstream of Great Slave Lake, were associated with the Interior platform, since  $>50\%$  of their catchment areas drain that region. The Mackenzie River itself has its entire course within the Interior Platform. The major axis regression model II was used to derive the function between  $\Delta^{14}\text{C}$ -DOC and  $\Delta^{14}\text{C}$ -POC, since this model allows both the explanatory and response variables to be treated as random. For all other regressions, a least squares model I was used. Relationships were considered significant when  $p$  values were  $<0.01$ . The South Nahanni river was excluded from regression models involving  $\Delta^{14}\text{C}$ -DOC, since this site was categorized as an outlier in three out of four models based on the analysis of Cook's distance (i.e.,  $>3$  times the mean Cook's D). All statistical analyses were performed on RStudio (R Core Team, 2020).

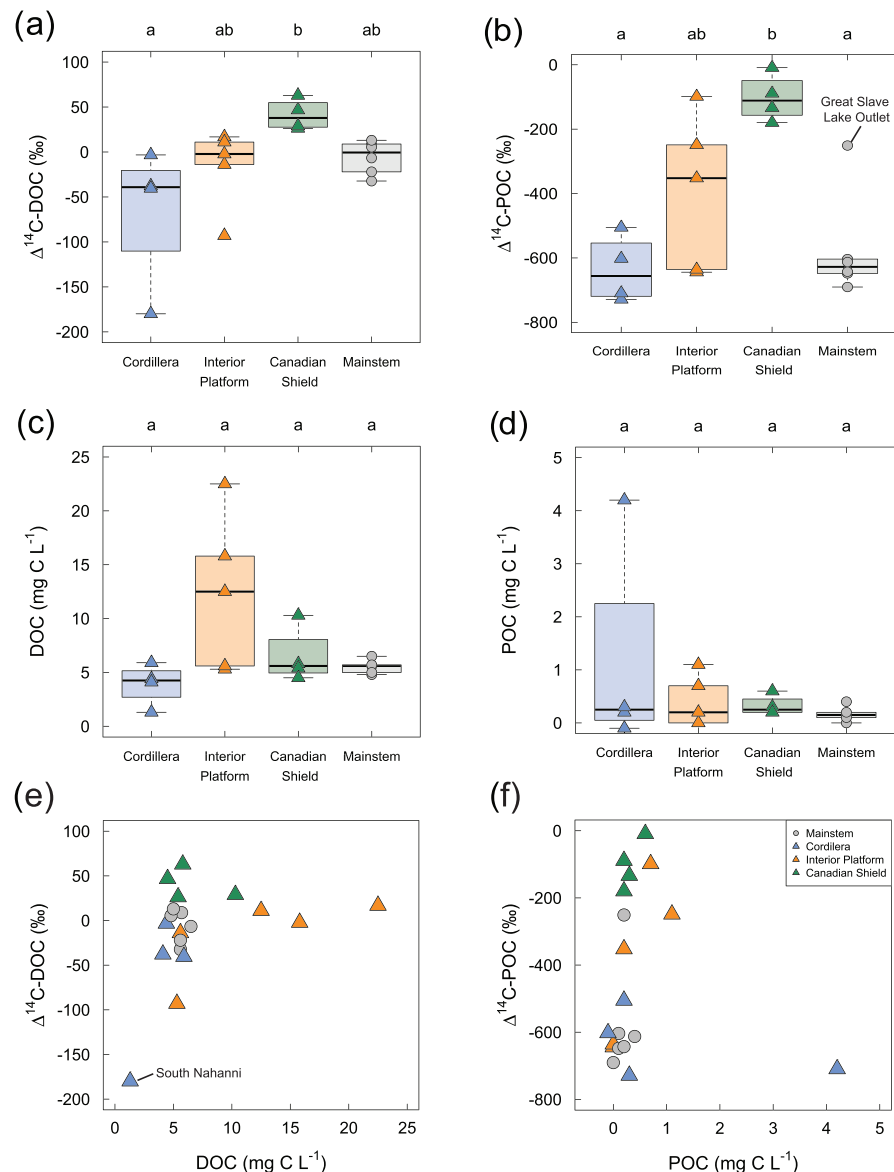


**Figure 2.** Boxplots summarizing the riverine (a)  $\Delta^{14}\text{C}$ -DOC, (b)  $\Delta^{14}\text{C}$ -POC, both in (‰), (c) DOC, and (d) POC concentration, both in ( $\text{mg C L}^{-1}$ ) for different tributaries ( $n = 14$ ) and the mainstem of the Mackenzie ( $n = 5$ ). The tributaries are grouped by their association with each geological province; Cordillera ( $n = 5$ ), Interior Platform ( $n = 5$ ), and Canadian Shield ( $n = 4$ ). The boxes represent the median, lower, and upper quartiles (25% and 75%) and the whiskers show the 5th and 95th percentiles. Specific values for each group are superimposed over the boxplot. The letters on the top  $x$  axis report the results from the pairwise Dunn's test, whereby different letters denote groups that were significantly different from each other. In (e) and (f) are scatterplots of the  $\Delta^{14}\text{C}$  content of (e) DOC and (f) POC as a function of their respective concentrations, with symbols following the same classification system as in other figures.

### 3. Results

#### 3.1. Isotopic Composition and Concentration of POC and DOC Across the MRB

The  $\Delta^{14}\text{C}$ -POC ranged from  $-728.8\text{‰}$  to  $-89.0\text{‰}$  across different locations, while the DOC was comparatively more  $^{14}\text{C}$  enriched, with values ranging from  $-179.9\text{‰}$  to  $62.9\text{‰}$  (Figures 1, 2a, and 2b). Rivers draining the Canadian Shield carried the most  $^{14}\text{C}$ -enriched DOC and POC, while  $^{14}\text{C}$ -depleted DOC and POC was more prevalent in the rivers draining the Cordillera (Figures 2a and 2b). This difference was statistically significant for rivers classified as draining the Cordillera and Canadian Shield, while rivers

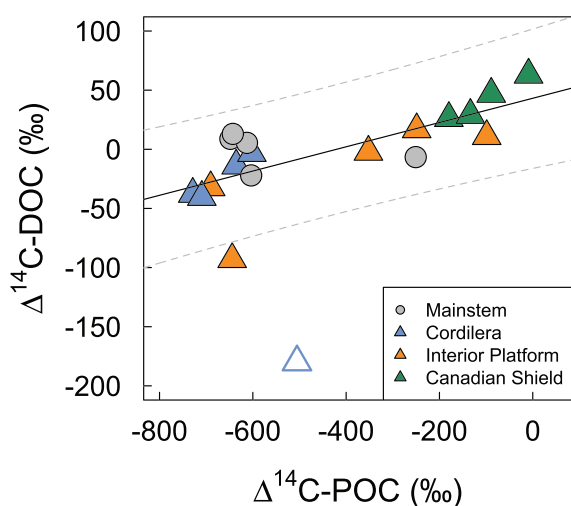


**Figure 3.** Scatterplot of  $\Delta^{14}\text{C-DOC}$  against  $\Delta^{14}\text{C-POC}$ , both in ‰, with the full line representing the linear regression model II and the 95% prediction intervals displayed with the gray dotted lines. The open triangle represents the South Nahanni River, which was excluded from the model based on the analysis of Cook's Distance.

classified as draining the Interior Platform reflected a mixture of the two neighboring geological regions (Figures 2a and 2b). These differences in the  $\Delta^{14}\text{C}$  of DOC and POC among these different groups of rivers were not reflected for the DOC and POC concentrations, which was comparatively more similar across rivers (Figures 2c and 2d). The DOC concentration across all different sampling locations ranged from 1.3 to 22.5 mg C L<sup>-1</sup>, while the POC concentration ranged from 0 to 4.2 mg C L<sup>-1</sup> (Figures 2c and 2d). The large majority of riverine OC was thus in DOC form (87–100%), with the exception of the Peel river, where the DOC share was only 58% of the total OC pool. There was no significant relationship between POC concentrations and  $\Delta^{14}\text{C-POC}$  ( $p = 0.7$ ) or between DOC concentrations and  $\Delta^{14}\text{C-DOC}$  across all river samples ( $p = 0.2$ ) (Figures 2e and 2f). The  $\delta^{13}\text{C}$  values of total OC for all rivers varies from  $-27.1\text{‰}$  to  $-25.6\text{‰}$ , which is representative of OC derived from C3 plants.

### 3.2. Controls on $\Delta^{14}\text{C-DOC}$ and $\Delta^{14}\text{C-POC}$ Spatial Variations

There was a significant positive linear relationship between the  $\Delta^{14}\text{C-POC}$  and  $\Delta^{14}\text{C-DOC}$  (Figure 3 and Table 1). Both  $\Delta^{14}\text{C-DOC}$  and  $\Delta^{14}\text{C-POC}$  were negatively related with turbidity, on log-scale, the stronger relationship being with  $\Delta^{14}\text{C-POC}$  ( $R^2 = 0.95$ ) (for  $\Delta^{14}\text{C-DOC}$ ,  $R^2 = 0.56$ ; Figures 4a and 4b and Table 1). Conversely, the relationship between turbidity and POC concentration was weak ( $R^2 = 0.3$ ), and not significant with DOC concentration ( $p = 0.2$ ).

There was a significant positive linear relationship between the  $\delta^{18}\text{O}$  value of water and both  $\Delta^{14}\text{C-DOC}$  and  $\Delta^{14}\text{C-POC}$  (Figures 4c and 4d and Table 1). The  $\delta^{18}\text{O}$  values of water ranged from  $-22.5\text{‰}$  to  $-13.3\text{‰}$ , with the most  $^{18}\text{O}$ -depleted values found in rivers associated with the Cordillera and the most  $^{18}\text{O}$ -enriched values observed in the Canadian Shield rivers (Figures 4c and 4d). There was no significant relationship between  $\delta^{18}\text{O}$  value of water and turbidity ( $R^2 = 0.03$ ,  $p = 0.30$ ). There was also no significant relationship between  $\Delta^{14}\text{C-DOC}$  or  $\Delta^{14}\text{C-POC}$  and dissolved or total nitrogen (DOC  $p = 0.3$ , POC  $p = 0.03$ ) or dissolved oxygen ( $\text{O}_2$ ) saturation (DOC  $p = 0.3$ , POC  $p = 0.03$ ). There were significant negative linear relationships between  $\Delta^{14}\text{C-POC}$  and conductivity, ( $p = 0.001$ ,  $R^2 = 0.45$ ), total alkalinity ( $p = 0.003$ ,  $R^2 = 0.37$ ),  $\text{Ca}^{2+}$  ( $p = 0.0007$ ,  $R^2 = 0.48$ ),  $\text{Mg}^{2+}$  ( $p = 0.004$ ,  $R^2 = 0.35$ ), and  $\text{SO}_4^{2-}$  ( $p = 0.006$ ,  $R^2 = 0.33$ ), albeit a lower explanatory power than the relationships established above (Table 1). These same variables had no significant explanatory power on the  $\Delta^{14}\text{C-DOC}$  ( $p > 0.01$ ) nor did other water chemistry variables included in this study.

Among the different geospatial variables derived for the MRB (listed in method section 2.4) the mean catchment elevation was the best predictor of  $\Delta^{14}\text{C-DOC}$  and  $\Delta^{14}\text{C-POC}$  in water, despite having a much lower explanatory power than relationships established with water chemistry variables ( $R^2 = 0.27$  and  $0.37$ , respectively; Figures 4e and 4f and Table 1).

The  $\delta^{18}\text{O}$  value of river water was significantly negatively related with the average catchment elevation as well ( $R^2 = 0.63$ ,  $p$  value  $< 0.0001$ ), but not turbidity ( $R^2 = 0.02$ ,  $p$  value  $= 0.29$ ).

## 4. Discussion

### 4.1. Spatial Patterns in Riverine $\Delta^{14}\text{C}$ of DOC and POC

Our survey confirmed the presence of aged DOC and POC (i.e.,  $^{14}\text{C}$  depleted) in many tributaries of the MRB during spring freshet. This aged OC was not confined to rivers draining areas with rapidly thawing permafrost (e.g., Peel and Arctic Red rivers) but was widespread in the basin, irrespective of latitude (Figure 1). Aged OC was particularly evident among rivers that are issued from the Cordillera (i.e., Peace, Liard, Peel, South Nahanni, and Arctic Red Rivers) (Figures 2a and 2b). This region contains both ancient petrogenic OC sources (e.g., kerogens) and also soils that store Holocene peat or plant detritus preserved in permafrost

**Table 1**

Results of Pairwise Regression Analyses of  $\Delta^{14}\text{C-POC}$  and  $\Delta^{14}\text{C-DOC}$  Against Other River Water or Catchment Properties

$x$	$y$	$\hat{m}$	$\hat{b}$	$R^2$	$p$ value	$n$
$\Delta^{14}\text{C-POC}$	$\Delta^{14}\text{C-DOC}$	0.1	42.8	0.54	0.0005	18
$\log(\text{Turb})$	$\Delta^{14}\text{C-POC}$	-6.7	-129.3	0.95	<0.0001	19
$\delta^{18}\text{O}$	$\Delta^{14}\text{C-POC}$	81.2	1071.3	0.65	<0.0001	19
Elevation	$\Delta^{14}\text{C-POC}$	-0.6	-40.1	0.37	0.003	19
$\log(\text{Turb})$	$\Delta^{14}\text{C-DOC}$	-14.1	45	0.56	0.0002	18
$\delta^{18}\text{O}$	$\Delta^{14}\text{C-DOC}$	10.3	187.4	0.45	0.001	18
Elevation	$\Delta^{14}\text{C-DOC}$	-0.1	57.9	0.28	0.0001	18

Note. For all regressions, a simple linear model of the form  $y = \hat{m}x + \hat{b}$  was applied, where  $\hat{m}$  and  $\hat{b}$  are estimates of the slope and intercept and the model's  $p$  value.

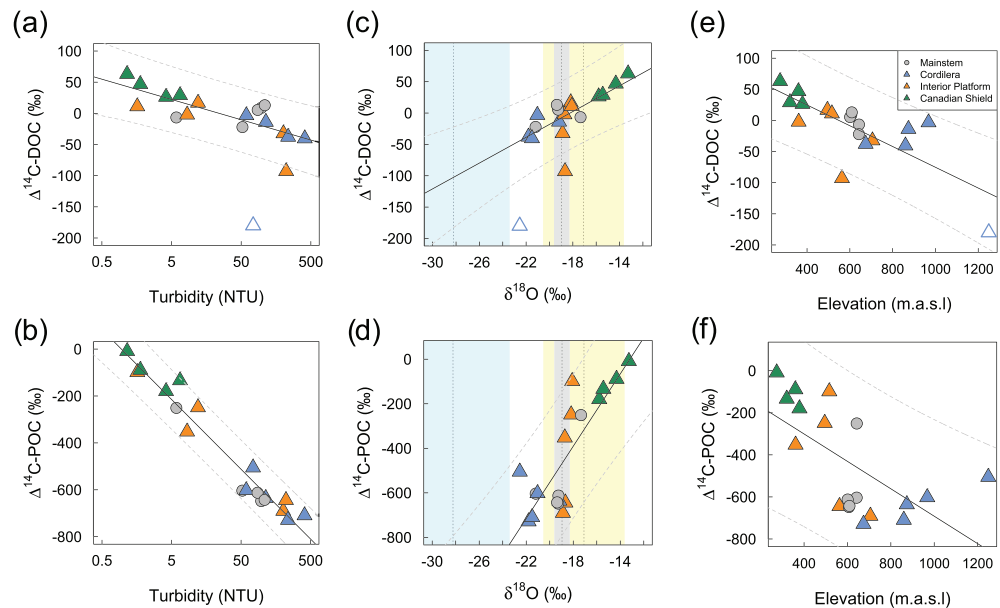


**Figure 4.** Riverine  $\Delta^{14}\text{C}$ -DOC and  $\Delta^{14}\text{C}$ -POC (both in ‰) as a function of (a and b) turbidity (NTU) on log scale, (c and d)  $\delta^{18}\text{O}$  of river water (‰), and (e and f) average catchment elevation in meters above sea level (m.a.s.l.). Triangles represent different tributaries and are colored based on their association to each geological province and grey circles represent the samples collected along the mainstem of the Mackenzie River. Full black lines represent the linear regression models with a 95% prediction interval represented with the gray dashed lines. The open triangle in (a), (c), and (e) identify the South Nahanni River, which was treated as an outlier in the regression models based on Cook's distance. In (c) and (d) various end-members for  $\delta^{18}\text{O}$  value of water are provided including; the mean annual  $\delta^{18}\text{O}$  value of water in the Mackenzie river at Tsiigehtchic with standard deviation (gray vertical line and rectangle respectively), the mean  $\delta^{18}\text{O}$  value of precipitation in June with standard deviation (yellow vertical line and rectangle respectively) and the mean  $\delta^{18}\text{O}$  value of snow with standard deviation (light cyan vertical line and rectangle, respectively) for all available measurement station in the region. The original  $\delta^{18}\text{O}$  values for these end-members is presented in Figure S5 and was obtained from GNIP and GNIR (Global network of Isotopes in Precipitation and in Rivers respectively).

(i.e., biogenic sources) (Figure S1 and Tables S1 and S4). Highly  $^{14}\text{C}$ -depleted OC of probable petrogenic origin has already been identified in rivers of the southern part of the MRB (Peace-Athabasca delta, which feeds the Slave River; Jautzy et al., 2015) and in the northmost tributaries draining the Cordillera (Liard, Peel and Arctic Red rivers; Hilton et al., 2015). Type III kerogens also make up a considerable share of the organic fraction of riverbank sediments along the Mackenzie River (Carrie et al., 2009). While petrogenic sources likely contribute aged-OC in these rivers, the supply from biogenic sources may be proportionally greater in the northmost rivers, which drain areas of ice-rich permafrost that are subject to rapidly growing retrogressive thaw slumps along riverbanks (Hilton et al., 2015; Kokelj et al., 2017; Littlefair et al., 2017).

Separating potential petrogenic and biogenic sources in this catchment based on geographical information is challenging, since they overlap considerably (Figure S1 and Tables S1 and S4). This mixture of OC sources in the MRB, comprising modern or old and petrogenic or biogenic sources, may explain the absence of clear connection with specific landscape variables included in our analysis (i.e., land cover class, permafrost cover, soil thickness, surficial materials and bedrock type). This diversity of OC sources is further emphasized by the lack of significant relationship between  $\Delta^{14}\text{C}$  and OC concentration for both DOC and POC fractions (Figures 2e and 2f). This precludes a simple mixing of two dominant OC sources, as reported for DOC in the Yukon River basin, where ancient DOC from glacial melt water and groundwater mixes with fresh and more abundant DOC in surface waters (Aiken et al., 2014). The  $\delta^{13}\text{C}$ -TOC values in our samples vary over a narrow range of values ( $-27.1\text{‰}$  to  $-26.5\text{‰}$ ) that confirms a C3-plant origin, from petrogenic or biogenic sources. The overlap between the  $\delta^{13}\text{C}$  values of these end-members forestalls a more precise estimate of their respective contributions (i.e.,  $\delta^{13}\text{C}_{\text{biogenic}}$   $-35\text{‰}$  to  $-21\text{‰}$  [Coplen et al., 2010] and  $\delta^{13}\text{C}_{\text{petrogenic}}$   $-28.9\text{‰}$  to  $28.5\text{‰}$  in the region [Johnston et al., 2012]). Findings from our  $\Delta^{14}\text{C}$  determinations,

nonetheless strengthen conclusions from earlier work to the effect that the old fraction of the OC exported by the MRB likely comprises a mixture of both petrogenic and biogenic sources (Goñi et al., 2005; Hilton et al., 2015; McClelland et al., 2016). A more detailed separation of the relative importance of petrogenic and biogenic OC sources in the MRB will be necessary to determine the role of riverine OC export in the contemporary C cycling.

Modern DOC (i.e.,  $^{14}\text{C}$ -enriched) and more recent POC was more prevalent in rivers draining the Canadian Shield (e.g., the Yellowknife, Snare, Cameron, and Marian Rivers; Figures 1, 2a, and 2b). This may arise from a lower input of aged-OC, caused by the smaller coverage of sedimentary rocks and thinner organic soil deposits in this region (Table S1 and Figure S1). Conversely, a predominant input of modern OC sources, derived from the forest vegetation or aquatic biomass in the numerous small lakes and wetlands dotting the region, could also contribute to these age patterns. The convergence of rivers draining the Cordillera, generally containing older OC fractions, with these of the Canadian Shield, generally exporting more modern OC fractions, corresponded well with the range in OC-ages observed along the Mackenzie River itself (Figures 2a and 2b), as well as those reported at the river mouth (Holmes et al., 2020) (Figure S4a).

#### 4.2. Coupling and Offset in the $\Delta^{14}\text{C}$ of DOC and POC

The range of  $\Delta^{14}\text{C}$ -DOC and  $\Delta^{14}\text{C}$ -POC reported here was large ( $\Delta^{14}\text{C}$ -POC  $-728.8\text{‰}$  to  $-89.0\text{‰}$  and  $\Delta^{14}\text{C}$ -DOC  $-179.9\text{‰}$  to  $62.9\text{‰}$ ,  $n = 19$ ) (Figures 2a and 2b). It spans nearly the full spectrum of values reported at the mouth of all Arctic Great Rivers ( $\Delta^{14}\text{C}$ -POC  $-674\text{‰}$  to  $-120\text{‰}$ ,  $n = 191$ , and  $\Delta^{14}\text{C}$ -DOC  $-185\text{‰}$  to  $152\text{‰}$ ,  $n = 133$ ; Holmes et al., 2020) and in other river basins worldwide ( $\Delta^{14}\text{C}$ -POC  $-956\text{‰}$  to  $139\text{‰}$ ,  $n = 532$  and  $\Delta^{14}\text{C}$ -DOC  $-453\text{‰}$  to  $336\text{‰}$ ,  $n = 696$ ; Marwick et al., 2015). Our spatial survey reveals a direct positive relationship between the  $\Delta^{14}\text{C}$  of DOC and POC across the MRB (Figure 3 and Table 1). This is surprising given that riverine DOC and POC are subject to important differences in transport pathways, reactivity and sources, thus usually resulting in considerable differences in their respective ages (Griffith et al., 2012; Guo et al., 2007; Marwick et al., 2015). The unusual coupling between the  $\Delta^{14}\text{C}$  of DOC and POC thus suggests some common landscape and/or hydrological control on the spatial distribution of both riverine OC sources in the MRB. To our knowledge, no similar relationships have been explicitly reported in other river catchments, except possibly in small tributaries of the Hudson River in the eastern USA, where ancient OC source are also present in the bedrock (Longworth et al., 2007). The relationship between the  $\Delta^{14}\text{C}$  of DOC and POC becomes less apparent in samples collected along the Mackenzie River itself (gray circles on Figure 3) nor is it observed in waters sampled at the mouth of the Mackenzie or in other Arctic Great Rivers (Figure S4a). This suggest that the mixing of waters issued from different tributaries could mask a broader spatial co-variation between  $\Delta^{14}\text{C}$ -DOC and  $\Delta^{14}\text{C}$ -POC in the MRB and potentially other Arctic Great Rivers as well. OC transformation along river networks, modulated by inter-regional differences in reactivity (Kaiser et al., 2017), may contribute to clouding these spatial co-variation in OC sources in larger river systems.

Besides the spatial co-variation, there was also a large and persistent offset between the  $\Delta^{14}\text{C}$  of DOC and POC across the MRB. The POC was systematically older (i.e., more  $^{14}\text{C}$ -depleted, by up to  $669\text{‰}$ ) when compared with DOC in the same waters. Similar differences have been reported in studies from rivers worldwide (Marwick et al., 2015; Mayorga et al., 2005; Raymond & Bauer, 2001b), as well as in other Arctic Great Rivers (Striegl et al., 2007; Wild et al., 2019). This age disparity reinforces earlier interpretations suggesting that POC is more associated with ancient soil C stocks, mobilized via thawing permafrost, river bank erosion and petrogenic OC sources, while DOC is derived, to a larger extent, from modern terrestrial and/or aquatic biomass (Guo et al., 2007; Holmes et al., 2020).

The non-conservative nature of POC and DOC during riverine transport, also imply that their  $\Delta^{14}\text{C}$  offset could reflect differences in their reactivity or transport pathway. Long water residence time in the MRB, extended by its many large lakes (Yi et al., 2010), provides opportunity for local transformation processes to occur (Catalán et al., 2016). Within the DOC pool, different size classes (e.g., colloidal and low/high molecular weight) can exhibit markedly different  $\Delta^{14}\text{C}$  contents suggesting potential differences in hydrodynamic sorting and reactivity, as exemplified in the neighboring Yukon river (Guo & Macdonald, 2006). To date, studies have not been conclusive as to the net effect of different transformation processes on the  $\Delta^{14}\text{C}$  of riverine OC, in part because OC reactivity can vary widely across regions (Kaiser et al., 2017). For

example, a growing body of evidence indicates that aged fractions of the DOC, of possible permafrost origin, remains highly bio-reactive during riverine transport (Mann et al., 2015; Vonk et al., 2013), but other studies report opposite effects (Dean et al., 2020; Drenzek et al., 2007; Goñi et al., 2005). Similar disagreements prevail in lower latitude catchments (e.g., Caraco et al., 2010; Dean et al., 2019; McCallister & del Giorgio, 2012) as opposed to, for example, Mayorga et al. (2005) and Raymond and Bauer (2001a). The reactivity of different POC age fraction is even more ambiguous, but binding to the abundant mineral particle load in the Mackenzie may help preserve POC during riverine transport (Carrie et al., 2009; Goñi et al., 2005; Vonk et al., 2010). Delayed filtration in several of our samples could have skewed the  $\Delta^{14}\text{C}$  of DOC and POC toward older or younger fractions, the effect of which remains unknown (Figure S3 and Table S2). It is, however, encouraging to note that there was no considerable differences in the  $\Delta^{14}\text{C}$  of DOC and POC, or OC concentrations for one sample with delayed filtration collected on the Mackenzie, compared with other samples along the mainstem (Figure S3).

Riverine transport also alters the fate of different age fractions of DOC and POC. Retrogressive thaw slumps, for example, have been found to decrease the yield of soil DOC, but are suspected to increase that of POC, as seen from total suspended solid measurements (Kokelj et al., 2005; Littlefair et al., 2017). The POC is also notably influenced by hydrodynamic sorting. This causes finer particles to travel near the channel surface and these tend to contain older POC fractions (Goni et al., 2006; Hilton et al., 2015; Vonk et al., 2010). Conversely, aquatic primary production may supply fresh DOC and POC near the channel surface, where light availability is greatest (Griffith et al., 2012; Tank et al., 2011). These various effects can cause considerable differences in the  $\Delta^{14}\text{C}$  content of DOC and POC with river depth. This points again to a potential source of uncertainty in our data. Depth-integrated sampling, not always comprising the deepest waters, and conducted mid-channel or sometimes offshore, could have introduced additional variability in the  $\Delta^{14}\text{C}$  of DOC and POC among these rivers (Figure S3 and Table S2). For now, these effects on the  $\Delta^{14}\text{C}$  remain unclear.

A considerable fraction of aged-DOC is transported across the MRB, for example, in the Arctic Red, Peel, Liard, Peace, and Slave Rivers. Distinctly old DOC was observed in the South Nahanni River ( $-179.9\text{‰}$ ), which drains part of the Liard River sub-basin within the Cordillera, and stood out as an outlier in the relationship with  $\Delta^{14}\text{C}$ -POC (Figure 3), turbidity and  $\delta^{18}\text{O}$  value of water (Figures 4a and 4c). This river is partly fed by alpine glaciers (Table S4: 0.5%, or  $\sim 183 \text{ km}^2$  in 2008; (Demuth et al., 2014)) (Figure S1a). Although they cover a small part of the catchment, they could represent an important source of aged-DOC, as demonstrated in glaciated parts of the Yukon River Basin (Aiken et al., 2014). The South Nahanni River also drains elevated uplands with limited forest productivity and thinner organic soils, which likely account for its particularly low DOC concentration ( $1.3 \text{ mg C L}^{-1}$ ) and potentially its unusually low  $\Delta^{14}\text{C}$  (Figure 2e). How representative are these DOC age patterns compared with the catchment's annual OC yield, and why these singularities in DOC sources are less pronounced for the POC, remains to be determined.

#### 4.3. Geomorphological and Hydrological Controls on Riverine OC Sources

Despite the large variability in the  $\Delta^{14}\text{C}$  of DOC and POC across the MRB, some consistent associations with water chemistry and catchment geomorphology were identified. These may provide clues on the controls of OC sources in the MRB. The negative relationship between turbidity and the  $\Delta^{14}\text{C}$  of both DOC and POC points to a predominantly terrestrial origin or control on riverine OC, particularly for POC (Figures 4a and 4b). The significant relationships between  $\Delta^{14}\text{C}$ -POC and soil weathering products (i.e., conductivity, alkalinity,  $\text{Ca}^{2+}$ ,  $\text{Mg}^{2+}$ , and  $\text{SO}_4^{2-}$ ) corroborates such terrestrial origin. All of these products have been shown to increase due to thermokarst thaw in this region (Kokelj et al., 2005). Interestingly, the turbidity of water in these rivers did not explain the concentration of OC, but only its age property. The turbidity of water can arise from fine sediment particles suspended in water, such as clay and silt derived from glacial sediments. In the case of the MRB, a larger contribution from these mineral-soil particles seems to correlate with older OC sources (Hilton et al., 2015), rather than the amount of OC. Fine sediment particles do not necessarily contain aged DOC and POC, but their abundance in rivers may indicate a greater physical soil erosion, which can co-mobilize old OC from organic soil (biogenic) or OC-rich rocks (petrogenic). A similar connection between sediment yield and  $\Delta^{14}\text{C}$ -POC was reported in mountainous river catchments at lower latitudes, where petrogenic OC sources were also present in the catchment geology (Leithold et al., 2006). The negative relationship between average catchment elevation and the  $\Delta^{14}\text{C}$  of

DOC and POC (Figures 4e and 4f) also points to an influence of geomorphology. Catchments of higher elevation and steeper slope, hence with faster-flowing rivers, appear more susceptible to mobilize aged OC. Seasonal monitoring at the mouth of the Mackenzie River reveals a similar negative relationship between  $\Delta^{14}\text{C}$ -POC and total suspended solid, which is not apparent at the mouth of other Arctic rivers, pointing again to the distinct character of the MRB (Figure S4e).

Alternatively, murky waters may be less productive due to light attenuation, thus decreasing the input of young DOC and POC. The lack of significant relationship between the  $\Delta^{14}\text{C}$  of DOC and POC and nitrogen or dissolved  $\text{O}_2$ , points to a relatively small control by instream primary production. However, for rivers heavily influenced by lakes, suspended algal material can be a proportionally greater source of POC and turbidity (Osburn et al., 2019). This was likely the case of the outlet of the Great Slave Lake, where POC was noticeably more recent ( $\Delta^{14}\text{C} -251\text{‰}$ ), compared with other locations along the Mackenzie River (Figure 2b). At a broader scale, more turbid waters would likely contain younger OC if algae-generated turbidity was predominant across the MRB, hence the opposite relationship to the one observed in our data. More detailed studies will be needed to shed light on the underlying mechanisms giving rise to these relationships.

The seasonality of air temperatures in the MRB causes large fluctuations in the  $\delta^{18}\text{O}$  value of precipitation, which varies between an average of  $-28.2 \pm 4.8\text{‰}$  in winter snowfall to  $-17.1 \pm 3.5\text{‰}$  in June rainfall, with an annual mean of  $-19.0\text{‰}$  over all available stations in the regions (Figures 4c and 4d and S5a). On account of this seasonality, the  $\delta^{18}\text{O}$  value of surface waters provides a tracer of water residence time at the catchment scale. Short catchment water residence time are indicated by rivers with  $\delta^{18}\text{O}$  values close to that of recent precipitation, while those supplied by well-mixed groundwater sources with longer residence time hold a more stable  $\delta^{18}\text{O}$  value that remains close to the mean annual precipitation value (Barnes et al., 2018; Peralta-Tapia et al., 2015; Tetzlaff et al., 2015). In high-latitude rivers, large snowmelt inputs during the spring freshet complicates this interpretation with a surge of  $^{18}\text{O}$ -depleted water during peak discharge (Lyon et al., 2010; Welp et al., 2005). In the MRB, the  $\Delta^{14}\text{C}$  of both DOC and POC increases significantly with the riverine  $\delta^{18}\text{O}$  value, which identifies a certain hydrological control on riverine OC sources (Figures 4c and 4d). This relationship could be explained by at least two different mechanisms: (1) a control by the catchment water residence time and flow path depth (e.g., Barnes et al., 2018) or (2) an effect of rising discharge associated with snowmelt during spring freshet (e.g., Welp et al., 2005).

Water isotope measurements in precipitation are scarce in this regions, with several measurements scattered across the latitude gradient, but only located in the eastern lowlands (e.g., stations elevation from 27 to 241 m.a.s.l; Figure S5a). This greatly complicates attempts to apportion and model spatial variations in snowmelt water contribution for different rivers in the MRB. Still, general associations to major  $\delta^{18}\text{O}$  end-members can be distinguished in our data. Rivers issued from the Cordillera had more  $^{18}\text{O}$ -depleted waters, with values closer to the isotopic ratio of snow (blue area in Figures 4c and 4d), and generally contained more  $\Delta^{14}\text{C}$ -depleted DOC and POC. Conversely, rivers located in the Canadian Shield contained more  $^{18}\text{O}$ -enriched waters, which resembles recent precipitation (yellow area in Figures 4c and 4d), and corresponded with more  $\Delta^{14}\text{C}$ -enriched DOC and POC. Other studies conducted in boreal headwater catchments have reported increases in the  $\Delta^{14}\text{C}$ -DOC during spring thaw, which is opposite to the relationship in our data (e.g., in peatlands [Campeau et al., 2017] and in forest soils [Campeau et al., 2019]). A similar increase in the  $\Delta^{14}\text{C}$ -DOC with more  $^{18}\text{O}$ -depleted waters occurs at the mouth of all Arctic Great Rivers, including the Mackenzie (Barnes et al., 2018; Figure S4b), which is again opposite to our data (Figure 4b). Glacial meltwater can export ancient DOC, as indicated in the Yukon River (Aiken et al., 2014), but these are typically associated with lower DOC concentrations, which is again inconsistent with our data. The relationship between river  $\delta^{18}\text{O}$  values and  $\Delta^{14}\text{C}$ -POC for the other Arctic Great Rivers is more consistent with ours than that for  $\Delta^{14}\text{C}$ -DOC (Barnes et al., 2018; Figure S4d). Still, such inconsistencies indicate that spatial variation in snowmelt water contribution is unlikely the sole driver causing the relationship between  $\delta^{18}\text{O}$  values and  $\Delta^{14}\text{C}$ -DOC and  $\Delta^{14}\text{C}$ -POC in these rivers.

The particularly close negative relationship between  $\delta^{18}\text{O}$  values and  $\Delta^{14}\text{C}$  of DOC and POC for the Canadian Shield tributaries ( $\Delta^{14}\text{C}$ -POC:  $R^2 = 0.96$ ,  $p = 0.01$  and  $\Delta^{14}\text{C}$ -DOC:  $R^2 = 0.99$ ,  $p = 0.002$ ; Figures 4c and 4d), where  $\delta^{18}\text{O}$  values in rivers were closer to that of recent precipitation, is an indication

## Acknowledgments

This project was funded by grant # 2017-00660 (P.I. C. Zdanowicz) from Formas, the Swedish government research council for sustainable development. Additional support from Formas through grant #2019-01529 (P.I. A. Campeau) is also acknowledged. River sampling in the Northwest Territories was conducted under a Scientific Research Licence issued by the Aurora Research Institute, and with the guidance and/or assistance of community residents and organizations of the following First Nation (FN) groups, to whom we are greatly indebted: South Slave Region: Fort Resolution Metis Council and Deninu K'ue FN (Fort Resolution), and Smith's Landing FN (Fort Smith); North Slave Region: North Slave Métis Alliance (Yellowknife) and Tłıchǫ Government (Behchokǫ); Deh Cho region: Deh Gah Gotie FN (Fort Providence), Łı́ldı́j Kų́ę FN (Fort Simpson), and Sambaa K'e FN (Sambaa K'e River); Mackenzie Delta region: Gwich'in Tribal Council (Inuvik) and Tetlit Gwich'Renewal Resources Council (Fort McPherson). In Inuvik, we also benefited from the support of the Western Arctic Research Center and its staff. Sampling on the Peace River in Wood Buffalo National Park, Alberta, was carried out under Park Canada research permit WB-2018-27981 and with kind permission from the Mikisew Cree First Nation. The Salt River FN also provided both guidance and access to the Peace River at Fort Fitzgerald. Hendrick Falk and Steve Kokelj (Northwest Territories Geological Survey) and Bruce Stuart (Taiga Environmental Laboratory) gave valuable advice or support in planning the field and lab work. Torbjörn Johannes Erikson and Emmanuel Queyla provided valuable assistance in the field. Analytical services in Ottawa were provided by Paul Middlestead, Wendi Abdi, and Patricia Wickham at the Jan Veizer Stable Isotope Laboratory, and by Carolyn Dziawa, Christabel Jean, Sarah Murseli, and Dr. Xiao-Lei Zhao at the A. E. Lalonde AMS Laboratory.

that the hydrological control on  $\Delta^{14}\text{C}$ -OC goes beyond just the influence of snowmelt. The relationships between riverine  $\delta^{18}\text{O}$  values,  $\Delta^{14}\text{C}$  of DOC and POC, and catchment elevation, could account for spatial variations in groundwater residence time and flow path depth, associated with different catchment geomorphology. Rivers in the Canadian Shield transport younger OC and waters with a  $\delta^{18}\text{O}$  value close to recent precipitation, indicating short water residence time with shallow flow paths (Figures 4c and 4d). This is consistent with the thin surface soil deposits in the region (Tables S1 and S4). It is possible that older riverine OC in rivers issued from the Cordillera could be mobilized by deeper groundwater flow paths with longer residence times. The low seasonality of  $\delta^{18}\text{O}$  values in the Liard and Mackenzie rivers supports well-mixed groundwater sources (Figure S5b). The steep topographic gradient of these rivers could make them more prone to riverbank erosion and may allow more hydrological contact with petrogenic OC sources in the bedrock or ancient peat buried in deeper soil layers.

The range in riverine  $\delta^{18}\text{O}$  values in our spatial survey ( $\delta^{18}\text{O}$  value  $-22.55\text{‰}$  to  $-13.27\text{‰}$ ) exceeds that measured at the mouth of the Mackenzie River (grey area on Figures 4c and 4d and S5b). Our data therefore capture local variations in catchment hydrology among different tributaries, which may be masked at the river mouth. Unlike in other Arctic Great Rivers, there is no consistent increase in DOC bioavailability and decrease in  $\Delta^{14}\text{C}$  with rising discharge during the spring freshet at the mouth of the Mackenzie River (Kaiser et al., 2017; Raymond et al., 2007). The important contrast in  $\Delta^{14}\text{C}$  of DOC and POC between the west and east bank of the MRB (Figures 2a and 2b) represents an additional complexity for characterizing the changes in OC sources in the MRB and how they mix during spring freshet. Finally, co-variation between many of the identified controls of riverine  $\Delta^{14}\text{C}$  of DOC and POC in this study highlights the need for future research to help disentangle these effects with a more detailed examination of the hydrological controls at play in the MRB.

## 5. Conclusions

This study provides a description and analysis of the spatial patterns in  $\Delta^{14}\text{C}$  of DOC and POC across large parts of the MRB. Collectively, our results demonstrate a remarkably large variability in riverine  $\Delta^{14}\text{C}$  of DOC and POC, but still a clear overlap in their respective sources and controls. This data reveals intriguing relationships between the  $\Delta^{14}\text{C}$  of DOC and POC and turbidity, water stable isotopes ratio and catchment elevation. Together, they suggest that hydrology and geomorphology are key to understanding riverine OC sources and their spatial controls in the MRB. Aged-OC is likely comprised of both petrogenic and biogenic sources, but these cannot be adequately separated and quantified here. The  $\Delta^{14}\text{C}$  patterns described here also seem to deviate considerably from those in other Arctic Great Rivers. While changes in catchment hydrology, in response to climate change, are anticipated across the circumpolar north (Peterson et al., 2002; Rood et al., 2017), these will likely have different implications for shifting riverine OC sources. Much of the underlying mechanisms giving rise to the relationships presented here are still ambiguous, thus establishing a need for more detailed examinations of the riverine OC sources and their controls in the MRB. The exact sources of riverine OC, their implication for the C cycle and potential to shift under further climate warming in this region, is still highly uncertain. Meanwhile, this study provides a road map of the key OC sources and their possible controls in this large and rapidly changing river basin.

## Conflict of Interest

The authors declare no conflict of interest.

## Data Availability Statement

Data are archived on the Bolin Center database (<https://doi.org/10.17043/campeau-2020>).

## References

- Abbott, B. W., Jones, J. B., Schuur, E. A. G., Chapin, F. S. III, Bowden, W. B., Bret-Harte, M. S., et al. (2016). Biomass offsets little or none of permafrost carbon release from soils, streams, and wildfire: An expert assessment. *Environmental Research Letters*, 11(3), 034014. <https://doi.org/10.1088/1748-9326/11/3/034014>
- Aiken, G. R., Spencer, R. G. M., Striegl, R. G., Schuster, P. F., & Raymond, P. A. (2014). Influences of glacier melt and permafrost thaw on the age of dissolved organic carbon in the Yukon River basin. *Global Biogeochemical Cycles*, 28, 525–537. <https://doi.org/10.1002/2013GB004764>

- Barnes, R. T., Butman, D. E., Wilson, H. F., & Raymond, P. A. (2018). Riverine export of aged carbon driven by flow path depth and residence time. *Environmental Science & Technology*, 52(3), 1028–1035. <https://doi.org/10.1021/acs.est.7b04717>
- Brown, J., Ferrians, O. J. Jr., Heginbottom, J. A., & Melnikov, E. S. (2002). Circum-Arctic map of permafrost and ground-ice conditions, *Report Rep. 45*, NSIDC: National Snow and Ice Data Center, Boulder, CO. <https://doi.org/10.3133/cp45>
- Burn, C. R., & Kokelj, S. V. (2009). The environment and permafrost of the Mackenzie Delta area. *Permafrost and Periglacial Processes*, 20(2), 83–105. <https://doi.org/10.1002/ppp.655>
- Bush, E., & Flato, G. M. (2019). Changes in Temperature and Precipitation in Canada: Chapter 4 in Canada's changing climate report *Rep.* (pp. 112–193). Government of Canada, Ottawa, Ontario.
- Cameron, A. R., & Beaton, A. P. (2000). Coal resources of Northern Canada with emphasis on Whitehorse Trough, Bonnet Plume Basin and Brackett Basin. Geological Survey of Canada Contribution No. 1999-127.1. *International Journal of Coal Geology*, 43(1–4), 187–210. [https://doi.org/10.1016/S0166-5162\(99\)00059-2](https://doi.org/10.1016/S0166-5162(99)00059-2)
- Campeau, A., Bishop, K., Amvrosiadi, N., Billett, M. F., Garnett, M. H., Laudon, H., et al. (2019). Current forest carbon fixation fuels stream CO<sub>2</sub> emissions. *Nature Communications*, 10(1), 1876. <https://doi.org/10.1038/s41467-019-09922-3>
- Campeau, A., Bishop, K. H., Billett, M. F., Garnett, M. H., Laudon, H., Leach, J. A., et al. (2017). Aquatic export of young dissolved and gaseous carbon from a pristine boreal fen: Implications for peat carbon stock stability. *Global Change Biology*, 23(12), 5523–5536. <https://doi.org/10.1111/gcb.13815>
- Caraco, N., Bauer, J. E., Cole, J. J., Petsch, S., & Raymond, P. (2010). Millennial-aged organic carbon subsidies to a modern river food web. *Ecology*, 91(8), 2385–2393. <https://doi.org/10.1890/09-0330.1>
- Carrie, J., Sanei, H., Goodarzi, F., Stern, G., & Wang, F. (2009). Characterization of organic matter in surface sediments of the Mackenzie River Basin, Canada. *International Journal of Coal Geology*, 77(3–4), 416–423. <https://doi.org/10.1016/j.coal.2008.03.007>
- Catalán, N., Marcé, R., Kothawala, D. N., & Tranvik, L. J. (2016). Organic carbon decomposition rates controlled by water retention time across inland waters. *Nature Geoscience*, 9(7), 501–504. <https://doi.org/10.1038/ngeo2720>
- Coplen, T. B., Hoppie, J. A., Böhlke, J. K., Peiser, H. S., Rieder, S. E., Krouse, H. R., et al. (2010). Compilation of minimum and maximum isotope ratios of selected elements in naturally occurring terrestrial materials and reagents, paper presented at Water-Resources Investigations Report 01-4222, U.S. Department of the Interior and U.S. Geological Survey.
- Crann, C. A., Murseli, S., St-Jean, G., Zhao, X., Clark, I. D., & Kieser, W. E. (2017). First status report on radiocarbon sample preparation techniques at the A.E. Lalonde AMS Laboratory (Ottawa, Canada). *Radiocarbon*, 59(3), 695–704. <https://doi.org/10.1017/RDC.2016.55>
- Davis, B. E. (2005). A guide to the proper selection and use of federally approved sediment and water-quality samplers *Rep.* (p. 20), Vicksburg, MS.
- Dean, J. F., Garnett, M. H., Spyarakos, E., & Billett, M. F. (2019). The potential hidden age of dissolved organic carbon exported by peatland streams. *Journal of Geophysical Research: Biogeosciences*, 124, 328–341. <https://doi.org/10.1029/2018JG004650>
- Dean, J. F., Meisel, O. H., Martyn Rosco, M., Marchesini, L. B., Garnett, M. H., Lenderink, H., et al. (2020). East Siberian Arctic inland waters emit mostly contemporary carbon. *Nature Communications*, 11(1), 1627. <https://doi.org/10.1038/s41467-020-15511-6>
- Demuth, M. N., Wilson, P., & Haggarty, D. (2014). Glaciers of the ragged range, Nahanni National Park Reserve, Northwest Territories, Canada. In J. S. Kargel, G. J. Leonard, M. P. Bishop, A. Kääb, B. H. Raup (Eds.), *Global Land Ice Measurements from Space* (pp. 375–383). Berlin Heidelberg, Berlin, Heidelberg: Springer. [https://doi.org/10.1007/978-3-540-79818-7\\_16](https://doi.org/10.1007/978-3-540-79818-7_16)
- Drenzek, N. J., Montluçon, D. B., Yunker, M. B., Macdonald, R. W., & Eglinton, T. I. (2007). Constraints on the origin of sedimentary organic carbon in the Beaufort Sea from coupled molecular <sup>13</sup>C and <sup>14</sup>C measurements. *Marine Chemistry*, 103(1–2), 146–162. <https://doi.org/10.1016/j.marchem.2006.06.017>
- Feng, X., Vonk, J. E., van Dongen, B. E., Gustafsson, O., Semiletov, I. P., Dudarev, O. V., et al. (2013). Differential mobilization of terrestrial carbon pools in Eurasian Arctic river basins. *Proceedings of the National Academy of Sciences of the United States of America*, 110(35), 14,168–14,173. <https://doi.org/10.1073/pnas.1307031110>
- Finstad, A. G., Andersen, T., Larsen, S., Tominaga, K., Blumentrath, S., de Wit, H. A., et al. (2016). From greening to browning: Catchment vegetation development and reduced S-deposition promote organic carbon load on decadal time scales in Nordic lakes. *Scientific Reports*, 6(1), 31944. <https://doi.org/10.1038/srep31944>
- Fulton, R. J. (2014). Surficial geology of Canada; Map 195 *Rep.* Geological Survey of Canada, Canadian Geoscience.
- Goni, M. A., Monacci, N., Gisewhite, R., Ogston, A., Crockett, J., & Nittrouer, C. (2006). Distribution and sources of particulate organic matter in the water column and sediments of the Fly River Delta, Gulf of Papua (Papua New Guinea). *Estuarine, Coastal and Shelf Science*, 69(1–2), 225–245. <https://doi.org/10.1016/j.ecss.2006.04.012>
- Goni, M. A., Yunker, M. B., Macdonald, R. W., & Eglinton, T. I. (2005). The supply and preservation of ancient and modern components of organic carbon in the Canadian Beaufort Shelf of the Arctic Ocean. *Marine Chemistry*, 93(1), 53–73. <https://doi.org/10.1016/j.marchem.2004.08.001>
- Gorham, E., Lehman, C., Dyke, A., Janssens, J., & Dyke, L. (2007). Temporal and spatial aspects of peatland initiation following deglaciation in North America. *Quaternary Science Reviews*, 26(3–4), 300–311. <https://doi.org/10.1016/j.quascirev.2006.08.008>
- Griffith, D. R., McNichol, A. P., Xu, L., McLaughlin, F. A., Macdonald, R. W., Brown, K. A., & Eglinton, T. I. (2012). Carbon dynamics in the western Arctic Ocean: Insights from full-depth carbon isotope profiles of DIC, DOC, and POC. *Biogeosciences*, 9(3), 1217–1224. <https://doi.org/10.5194/bg-9-1217-2012>
- Guay, K. C., Beck, P. S., Berner, L. T., Goetz, S. J., Baccini, A., & Buermann, W. (2014). Vegetation productivity patterns at high northern latitudes: A multi-sensor satellite data assessment. *Global Change Biology*, 20(10), 3147–3158. <https://doi.org/10.1111/gcb.12647>
- Guo, L., & Macdonald, R. W. (2006). Source and transport of terrigenous organic matter in the upper Yukon River: Evidence from isotope (<sup>δ</sup><sup>13</sup>C, <sup>Δ</sup><sup>14</sup>C, and <sup>δ</sup><sup>15</sup>N) composition of dissolved, colloidal, and particulate phases. *Global Biogeochemical Cycles*, 20, GB2011. <https://doi.org/10.1029/2005GB002593>
- Guo, L., Ping, C.-L., & Macdonald, R. W. (2007). Mobilization pathways of organic carbon from permafrost to arctic rivers in a changing climate. *Geophysical Research Letters*, 34, L13603. <https://doi.org/10.1029/2007GL030689>
- Hilton, R. G., Galy, V., Gaillardet, J., Dellinger, M., Bryant, C., O'Regan, M., et al. (2015). Erosion of organic carbon in the Arctic as a geological carbon dioxide sink. *Nature*, 524(7563), 84–87. <https://doi.org/10.1038/nature14653>
- Holmes, R. M., McClelland, J. W., Tank, S. E., Spencer, R. G. M., & Shiklomanov, A. I. (2020). Arctic Great Rivers Observatory. Water Quality Dataset, Version 20181010. Retrieved from <https://www.arcticgreatrivers.org/data>
- Horan, K., Hilton, R. G., Dellinger, M., Tipper, E., Galy, V., Calmels, D., et al. (2019). Carbon dioxide emissions by rock organic carbon oxidation and the net geochemical carbon budget of the Mackenzie River Basin. *American Journal of Science*, 319(6), 473–499. <https://doi.org/10.2475/06.2019.02>

- Jautzy, J. J., Ahad, J. M., Hall, R. I., Wiklund, J. A., Wolfe, B. B., Gobeil, C., & Savard, M. M. (2015). Source apportionment of background PAHs in the Peace-Athabasca Delta (Alberta, Canada) using molecular level radiocarbon analysis. *Environmental Science & Technology*, 49(15), 9056–9063. <https://doi.org/10.1021/acs.est.5b01490>
- Johnston, D. T., Macdonald, F. A., Gill, B. C., Hoffman, P. F., & Schrag, D. P. (2012). Uncovering the Neoproterozoic carbon cycle. *Nature*, 483(7389), 320–323. <https://doi.org/10.1038/nature10854>
- Kaiser, K., Canedo-Oropeza, M., McMahon, R., & Amon, R. M. W. (2017). Origins and transformations of dissolved organic matter in large Arctic rivers. *Scientific Reports*, 7(1), 13064. <https://doi.org/10.1038/s41598-017-12729-1>
- Kokelj, S. V., Jenkins, R. E., Milburn, D., Burn, C. R., & Snow, N. (2005). The influence of thermokarst disturbance on the water quality of small upland lakes, Mackenzie Delta region, Northwest Territories, Canada. *Permafrost and Periglacial Processes*, 16(4), 343–353. <https://doi.org/10.1002/ppp.536>
- Kokelj, S. V., Lantz, T. C., Tunnicliffe, J., Segal, R., & Lacelle, D. (2017). Climate-driven thaw of permafrost preserved glacial landscapes, northwestern Canada. *Geology*, 45(4), 371–374. <https://doi.org/10.1130/g38626.1>
- Lacelle, D., Brooker, A., Fraser, R. H., & Kokelj, S. V. (2015). Distribution and growth of thaw slumps in the Richardson Mountains–Peel Plateau region, northwestern Canada. *Geomorphology*, 235, 40–51. <https://doi.org/10.1016/j.geomorph.2015.01.024>
- Lang, S. Q., McIntyre, C. P., Bernasconi, S. M., Früh-Green, G. L., Voss, B. M., Eglinton, T. I., & Wacker, L. (2016). Rapid  $^{14}\text{C}$  analysis of dissolved organic carbon in non-saline waters. *Radiocarbon*, 58(3), 505–515. <https://doi.org/10.1017/RDC.2016.17>
- Lantz, T. C., & Kokelj, S. V. (2008). Increasing rates of retrogressive thaw slump activity in the Mackenzie Delta region, N.W.T., Canada. *Geophysical Research Letters*, 35, L06502. <https://doi.org/10.1029/2007GL032433>
- Latifovic, R., Pouliot, D., & Olthof, I. (2017). Circa 2010 land cover of Canada: Local optimization methodology and product development. *Remote Sensing*, 9(11), 1098. <https://doi.org/10.3390/rs9111098>
- Leithold, E. L., Blair, N. E., & Perkey, D. W. (2006). Geomorphologic controls on the age of particulate organic carbon from small mountainous and upland rivers. *Global Biogeochemical Cycles*, 20, GB3022. <https://doi.org/10.1029/2005GB002677>
- Lis, G., Wassenaar, L., & Hendry, M. (2008). High-precision laser spectroscopy D/H and  $^{18}\text{O}/^{16}\text{O}$  measurements of microliter natural water samples. *Analytical Chemistry*, 80(1), 287–293. <https://doi.org/10.1021/ac701716q>
- Littlefair, C. A., Tank, S. E., & Kokelj, S. V. (2017). Retrogressive thaw slumps temper dissolved organic carbon delivery to streams of the Peel Plateau, NWT, Canada. *Biogeosciences*, 14(23), 5487–5505. <https://doi.org/10.5194/bg-14-5487-2017>
- Longworth, B. E., Petsch, S. T., Raymond, P. A., & Bauer, J. E. (2007). Linking lithology and land use to sources of dissolved and particulate organic matter in headwaters of a temperate, passive-margin river system. *Geochimica et Cosmochimica Acta*, 71(17), 4233–4250. <https://doi.org/10.1016/j.gca.2007.06.056>
- Lyon, S. W., Laudon, H., Seibert, J., Mörth, M., Tetzlaff, D., & Bishop, K. H. (2010). Controls on snowmelt water mean transit times in northern boreal catchments. *Hydrological Processes*, 24(12), 1672–1684. <https://doi.org/10.1002/hyp.7577>
- Mann, P. J., Eglinton, T. I., McIntyre, C. P., Zimov, N., Davydova, A., Vonk, J. E., et al. (2015). Utilization of ancient permafrost carbon in headwaters of Arctic fluvial networks. *Nature Communications*, 6(1), 7856. <https://doi.org/10.1038/ncomms8856>
- Marwick, T. R., Tammooh, F., Teodoru, C. R., Borges, A. V., Darchambeau, F., & Bouillon, S. (2015). The age of river-transported carbon: A global perspective. *Global Biogeochemical Cycles*, 29, 122–137. <https://doi.org/10.1002/2014GB004911>
- Mayorga, E., Aufdenkampe, A. K., Masiello, C. A., Krusche, A. V., Hedges, J. I., Quay, P. D., et al. (2005). Young organic matter as a source of carbon dioxide outgassing from Amazonian rivers. *Nature*, 436(7050), 538–541. <https://doi.org/10.1038/nature03880>
- McCallister, S. L., & del Giorgio, P. A. (2012). Evidence for the respiration of ancient terrestrial organic C in northern temperate lakes and streams. *Proceedings of the National Academy of Sciences*, 109(42), 16,963–16,968. <https://doi.org/10.1073/pnas.1207305109>
- McClelland, J. W., Holmes, R. M., Peterson, B. J., Raymond, P. A., Striegl, R. G., Zhulidov, A. V., et al. (2016). Particulate organic carbon and nitrogen export from major Arctic rivers. *Global Biogeochemical Cycles*, 30, 629–643. <https://doi.org/10.1002/2015GB005351>
- Osburn, C. L., Anderson, N. J., Leng, M. J., Barry, C. D., & Whiteford, E. J. (2019). Stable isotopes reveal independent carbon pools across an Arctic hydro-climatic gradient: Implications for the fate of carbon in warmer and drier conditions. *Limnology and Oceanography Letters*, 4(6), 205–213. <https://doi.org/10.1002/lol2.10119>
- Pelletier, J. D., Broxton, P. D., Hazenberg, P., Zeng, X., Troch, P. A., Niu, G. Y., et al. (2016). A gridded global data set of soil, intact regolith, and sedimentary deposit thicknesses for regional and global land surface modeling. *Journal of Advances in Modeling Earth Systems*, 8, 41–65. <https://doi.org/10.1002/2015MS000526>
- Peralta-Tapia, A., Sponseller, R. A., Ågren, A., Tetzlaff, D., Soulsby, C., & Laudon, H. (2015). Scale-dependent groundwater contributions influence patterns of winter baseflow stream chemistry in boreal catchments. *Journal of Geophysical Research: Biogeosciences*, 120, 847–858. <https://doi.org/10.1002/2014JG002878>
- Peterson, B. J., Holmes, R. M., McClelland, J. W., Vorosmarty, C. J., Lammers, R. B., Shiklomanov, A. I., et al. (2002). Increasing river discharge to the Arctic Ocean. *Science*, 298(5601), 2171–2173. <https://doi.org/10.1126/science.1077445>
- Qian, H., Joseph, R., & Zeng, N. (2010). Enhanced terrestrial carbon uptake in the Northern High Latitudes in the 21st century from the Coupled Carbon Cycle Climate Model Intercomparison Project model projections. *Global Change Biology*, 16(2), 641–656. <https://doi.org/10.1111/j.1365-2486.2009.01989.x>
- R Core Team (2020). *R: A language and environment for statistical computing*. Vienna, Austria: R Foundation for Statistical Computing. <http://www.R-project.org/>
- Ramsey, C. B. (2009). Bayesian analysis of radiocarbon dates. *Radiocarbon*, 51(1), 337–360. <https://doi.org/10.1017/S0033822200033865>
- Raymond, P. A., & Bauer, J. E. (2001a). Riverine export of aged terrestrial organic matter to the North Atlantic Ocean. *Nature*, 409(6819), 497–500. <https://doi.org/10.1038/35054034>
- Raymond, P. A., & Bauer, J. E. (2001b). Use of  $^{14}\text{C}$  and  $^{13}\text{C}$  natural abundances for evaluating riverine, estuarine, and coastal DOC and POC sources and cycling: A review and synthesis. *Organic Geochemistry*, 32(4), 469–485. [https://doi.org/10.1016/S0146-6380\(00\)00190-X](https://doi.org/10.1016/S0146-6380(00)00190-X)
- Raymond, P. A., McClelland, J. W., Holmes, R. M., Zhulidov, A. V., Mull, K., Peterson, B. J., et al. (2007). Flux and age of dissolved organic carbon exported to the Arctic Ocean: A carbon isotopic study of the five largest arctic rivers. *Global Biogeochemical Cycles*, 21, GB4011. <https://doi.org/10.1029/2007GB002934>
- Rice, E. W., Baird, R. B., & Eaton, A. D. E. (2017). *Standard methods for the examination of water and wastewater Method 2540 D. Total suspended solids* (23rd ed., p. 1796). Washington, DC: American Public Health Association (APHA), American Water Works Association (AWWA), Water Environment Federation (WEF).
- Roberts, M. L., Elder, K. L., Jenkins, W. J., Gagnon, A. R., Xu, L., Hlavenka, J. D., & Longworth, B. E. (2019).  $^{14}\text{C}$  Blank Corrections for 25–100  $\mu\text{g}$  Samples at the National Ocean Sciences AMS Laboratory. *Radiocarbon*, 61(5), 1403–1411. <https://doi.org/10.1017/RDC.2019.74>

- Rood, S. B., Kaluthota, S., Philipsen, L. J., Rood, N. J., & Zanewich, K. P. (2017). Increasing discharge from the Mackenzie River system to the Arctic Ocean. *Hydrological Processes*, 31(1), 150–160. <https://doi.org/10.1002/hyp.10986>
- St. Jacques, J.-M., & Sauchyn, D. J. (2009). Increasing winter baseflow and mean annual streamflow from possible permafrost thawing in the Northwest Territories, Canada. *Geophysical Research Letters*, 36, L01401. <https://doi.org/10.1029/2008GL035822>
- Stein, R., & Macdonald, R. W. (2004). *The organic carbon cycle in the Arctic Ocean*. Berlin Heidelberg: Springer-Verlag. <https://doi.org/10.1007/978-3-642-18912-8>
- St-Jean, G. (2003). Automated quantitative and isotopic ( $^{13}\text{C}$ ) analysis of dissolved inorganic carbon and dissolved organic carbon in continuous-flow using a total organic carbon analyser. *Rapid Communications in Mass Spectrometry*, 17(5), 419–428. <https://doi.org/10.1002/rcm.926>
- St-Jean, G., Kieser, W. E., Crann, C. A., & Murseli, S. (2017). Semi-automated equipment for  $\text{CO}_2$  purification and graphitization at the AE Lalonde AMS Laboratory (Ottawa, Canada). *Radiocarbon*, 59(3), 941–956. <https://doi.org/10.1017/RDC.2016.57>
- Striegl, R. G., Dornblaser, M. M., Aiken, G. R., Wickland, K. P., & Raymond, P. A. (2007). Carbon export and cycling by the Yukon, Tanana, and Porcupine rivers, Alaska, 2001–2005. *Water Resources Research*, 43, W02411. <https://doi.org/10.1029/2006WR005201>
- Stuiver, M., & Polach, H. A. (1977). Discussion; reporting of C-14 data. *Radiocarbon*, 19(3), 355–363. <https://doi.org/10.1017/S0033822200003672>
- Tank, S. E., Lesack, L. F. W., Gareis, J. A. L., Osburn, C. L., & Hesslein, R. H. (2011). Multiple tracers demonstrate distinct sources of dissolved organic matter to lakes of the Mackenzie Delta, western Canadian Arctic. *Limnology and Oceanography*, 56(4), 1297–1309. <https://doi.org/10.4319/lo.2011.56.4.1297>
- Tank, S. E., Striegl, R. G., McClelland, J. W., & Kokelj, S. V. (2016). Multi-decadal increases in dissolved organic carbon and alkalinity flux from the Mackenzie drainage basin to the Arctic Ocean. *Environmental Research Letters*, 11(5), 054015. <https://doi.org/10.1088/1748-9326/11/5/054015>
- Tetzlaff, D., Buttle, J., Carey, S. K., McGuire, K., Laudon, H., & Soulsby, C. (2015). Tracer-based assessment of flow paths, storage and runoff generation in northern catchments: A review. *Hydrological Processes*, 29(16), 3475–3490. <https://doi.org/10.1002/hyp.10412>
- Treat, C. C., & Jones, M. C. (2018). Near-surface permafrost aggradation in Northern Hemisphere peatlands shows regional and global trends during the past 6000 years. *The Holocene*, 28(6), 998–1010. <https://doi.org/10.1177/0959683617752858>
- Vonk, J. E., Giosan, L., Blusztajn, J., Montlucon, D., Graf Pannatier, E., McIntyre, C., et al. (2015). Spatial variations in geochemical characteristics of the modern Mackenzie Delta sedimentary system. *Geochimica et Cosmochimica Acta*, 171, 100–120. <https://doi.org/10.1016/j.gca.2015.08.005>
- Vonk, J. E., Mann, P. J., Davydov, S., Davydova, A., Spencer, R. G. M., Schade, J., et al. (2013). High biolability of ancient permafrost carbon upon thaw. *Geophysical Research Letters*, 40, 2689–2693. <https://doi.org/10.1002/grl.50348>
- Vonk, J. E., Sánchez-García, L., Semiletov, I., Dudarev, O., Eglinton, T., Andersson, A., & Gustafsson, Ö. (2010). Molecular and radiocarbon constraints on sources and degradation of terrestrial organic carbon along the Kolyma paleoriver transect, East Siberian Sea. *Biogeosciences*, 7(10), 3153–3166. <https://doi.org/10.5194/bg-7-3153-2010>
- Welp, L. R., Randerson, J. T., Finlay, J. C., Davydov, S. P., Zimova, G. M., Davydova, A. I., & Zimov, S. A. (2005). A high-resolution time series of oxygen isotopes from the Kolyma River: Implications for the seasonal dynamics of discharge and basin-scale water use. *Geophysical Research Letters*, 32, L14401. <https://doi.org/10.1029/2005GL022857>
- Wheeler, J. O., Hoffman, P. F., Card, K. D., Davidson, A., Sanford, B. V., Okulitch, A. V., & Roest, W. R. (1996). Geological map of Canada “A” series map 1860A, Rep.
- Wild, B., Andersson, A., Broder, L., Vonk, J., Hugelius, G., McClelland, J. W., et al. (2019). Rivers across the Siberian Arctic unearth the patterns of carbon release from thawing permafrost. *Proceedings of the National Academy of Sciences of the United States of America*, 116(21), 10,280–10,285. <https://doi.org/10.1073/pnas.1811797116>
- Xu, J., Morris, P. J., Liu, J., & Holden, J. (2018). PEATMAP: Refining estimates of global peatland distribution based on a meta-analysis. *Catena*, 160, 134–140. <https://doi.org/10.1016/j.catena.2017.09.010>
- Yi, Y., Gibson, J. J., Hélie, J.-F., & Dick, T. A. (2010). Synoptic and time-series stable isotope surveys of the Mackenzie River from Great Slave Lake to the Arctic Ocean, 2003 to 2006. *Journal of Hydrology*, 383(3–4), 223–232. <https://doi.org/10.1016/j.jhydrol.2009.12.038>
- Zhou, Y., Guo, H., Lu, H., Mao, R., Zheng, H., & Wang, J. (2015). Analytical methods and application of stable isotopes in dissolved organic carbon and inorganic carbon in groundwater. *Rapid Communications in Mass Spectrometry*, 29(19), 1827–1835. <https://doi.org/10.1002/rcm.7280>